Biomechanics and Modeling in Mechanobiology
https://doi.org/10.1007/s10237-019-01159-9

ORIGINAL PAPER

A multiscale synthesis: characterizing acute cartilage failure under an aggregate tibiofemoral joint loading

Malek Adouni[1,2,3] · Tanvir R. Faisal[1,2] · Mohamed Gaith[4] · Yasin Y. Dhaher[5,6,7]

Received: 19 June 2018 / Accepted: 26 April 2019

Abstract

Knee articular cartilage is characterized by a complex mechanical behavior, posing a challenge to develop an efficient and precise model. We argue that the cartilage damage, in general, can be traced to the fibril level as a plastic deformation, defined as micro-defects. To investigate these micro-defects, we have developed a detailed finite element model of the entire healthy tibiofemoral joint (TF) including a multiscale constitutive model which considers the structural hierarchies of the articular cartilage. The net model was simulated under physiological loading conditions to predict joint response under 2000 N axial compression and damage initiation under high axial loading (max 7 KN) when the TF joint flexed to 30°. Computed results sufficiently agreed with earlier experimental and numerical studies. Further, initiation and propagation of damage in fibrils were computed at the tibial cartilage located mainly in the superficial and middle layers. Our simulation results also indicated that the stiffer the fibril is (higher cross-link densities), the higher the contact stress required to elicit a fibril yield and the higher the rate of yielding as a function of increased contact stress. To the best of our knowledge, this is the first model that combines macro-continuum joint mechanics and micromechanics at the tissue level. The computational construct presented here serves as a simulation platform to explore the interplay between acute cartilage damage and micromechanics characteristics at the tropocollagen level.

Keywords Multiscale model · Tropocollagen · Fibrils · Cartilage damage · Tibiofemoral joint

1 Introduction

Knee joint articular cartilage experiences significant mechanical loads during activities of daily living and plays a key role in transferring and distributing loads through and within the tibiofemoral (TF) joint (Mow et al. 1980). At the tissue level, the cartilage consists of a meshwork of collagen II fibrils embedded in proteoglycans and water with a depth-dependent structure in which the fibrils have different spatial orientations. In the deep zone, the collagen fibrils are perpendicular to the subchondral bone and curve gradually (mid zone) to merge parallel (superficial zone) to the surface (Bi et al. 2005; Julkunen et al. 2008a). The organization of collagen and its architecture have been considered critical to the aggregate biomechanical response of the cartilage (Mononen et al. 2011; Shirazi et al. 2008; Wilson et al. 2004). Degeneration (mechanically or enzymatically mediated) of these fibrils will lead to acute and focal cartilage collapse (Bank et al. 2000; Maroudas et al. 1968; Wilson et al. 2006). While acute focal injuries to the cartilage are initially often asymptomatic, repeated injury can result in incremental damage,

Electronic supplementary material The online version of this article (https://doi.org/10.1007/s10237-019-01159-9) contains supplementary material, which is available to authorized users.

✉ Malek Adouni
malek.adouni@northwestern.edu; malek.adouni@gmail.com

1 Physical Medicine and Rehabilitation Department, Northwestern University, 345 East Superior Street, Chicago, IL 60611, USA

2 Legs + Walking Lab, Shirley Ryan AbilityLab, 355 East Erie, Chicago, IL 60611, USA

3 Mechanical Engineering Department, Australian College of Kuwait, P.O. Box 1411, East Mishref, Kuwait

4 Faculty of Engineering Technology, Al-Balqa Applied University, Amman 11171, Jordan

5 Department of Physical Medicine and Rehabilitation, University of Texas Southwest, Dallas, TX, USA

6 Department of Orthopedic Surgery, University of Texas Southwest, Dallas, TX, USA

7 Bioengineering, University of Texas Southwest, Dallas, TX, USA

Published online: 08 May 2019

greatly magnifying the potential for long-term complication. Indeed, recent studies have shown that cartilage injuries and degenerative disease in the USA are the primary sources of long-term disability (Barbour et al. 2017; Wallace et al. 2017).

The severity of the initial injury and treatment are important considerations that affect physical function. Identifying the nature of the correlation between damage at the fibril level, defined here as micro-defects, and cartilage loading can help elucidate the biochemical and mechanical interactions between aggregate loading levels and acute joint injury (Buehler and Ballarini 2013). However, experimental examinations in vivo on the interplay between full joint loading, cartilage degradation and tissue-level mechanics are technically prohibitive in humans and very limited in animal models, such as Abusara et al. (2011) where they have investigated the interplay between the cartilage loading and chondrocytes mechanics. Because human in vivo studies examining cartilage loading directly are not feasible, biomechanical experimental and modeling investigations are often used to study the aggregate joint kinematics and loading in normative or altered states (Adouni et al. 2012; Astephen 2007).

Cartilage has largely been historically represented as either a biphasic material composed of both solid and interstitial fluid phases (Mononen et al. 2012; Mow et al. 1980) or a solid phase with either linear or nonlinear elastic mechanical characteristics (Adouni and Shirazi-Adl 2009; Adouni et al. 2012; Pena et al. 2005; Shirazi et al. 2008). Both constructs ignore the simultaneous expression of the depth-dependent morphological features of cartilage, including the orientation of the collagen fibrils (Julkunen et al. 2008b) and the elasto-plastic mechanics of the fibril level (tropocollagen cross-links levels) at which cartilage failure is expressed. At the microscopic level, cartilage tensile stiffness appears to depend primarily on the cross-link density between the tropocollagen molecules, key contributors to matrix integrity (Fratzl 2008). Animal studies have shown a strong correlation between collagen cross-link density and tensile stiffness/strength in bovine articular cartilage (Kaukinen et al. 2005). In recent years, molecular dynamics simulations at the fibril level have shown a strong inverse association between the fibril strength and cross-link density across tropocollagen molecules (Buehler 2006; Malaspina et al. 2017).

Indeed, soft biological tissues can be manipulated as hyper-deformable fiber-reinforced composite structures (Holzapfel et al. 2000). From an engineering point of view, it is well recognized that biological tissues undergo plastic deformations when loaded beyond the physiological range. This kind of soft tissue was well characterized by typical yielding and failure regions associated with an irreversible increase in its length. The yielding and post-yielding behavior was well explained by a relative slip between collagen molecules (chains), a mechanism of damage-based softening plastic deformation (Abrahams 1967; Gasser and Holzapfel 2002; Holzapfel et al. 2000; Kaukinen et al. 2005; Tang et al. 2010; Schmidt-Baldassari 2003; Sverdlik and Lanir 2002).

Accordingly, we seek to develop a multiscale constitutive model of cartilage, incorporating the structural hierarchies of this tissue and its molecular constructs (tropocollagen–fibril) coupled with a finite element model of the human tibiofemoral joint. Our computational framework will employ a recently developed multilayered, fibril-reinforced, multiscale cartilage model (Adouni and Dhaher 2016). This model has been statistically calibrated and extensively validated, verified and cross-verified against available experimental data. The model will help capture the intricate and full path of articular cartilage fibrils damage from pre-yield to post-yield states under loading conditions synonymous with loads experienced during certain activities of daily living (Meyer et al. 2008; Mokhtarzadeh et al. 2013). The identification of a micro-cartilage defect can be a key indicator of the initiation of osteoarthritis demonstrated by decreased turnover of collagen in cartilage (Tiku and Madhan 2016). Hence, awareness of the primary collagen defect as a function of mechanical overcapacity may help to predict pathological progression at an earlier stage and advance selection and effectiveness of patient-specific interventions, which is currently challenging (Kraus et al. 2015).

2 Methods

2.1 Finite element (FE) model

A validated finite element model to predict the TF joint response that consists of all the relevant soft tissues has been considered in the current work. The detailed description of the FE model was demonstrated in prior work (Dhaher et al. 2010; Schroeder 2010, 2014) (details also included in Supplementary Materials), and only a brief overview will be described here. The tibiofemoral model included two bony structures—tibia and femur—which were simulated as rigid bodies with much higher stiffness in comparison with associated soft tissues such as ligaments, articular cartilage and menisci (Donahue et al. 2002). Continuum-based reduced integration hexahedral elements were used to model the articular cartilage, menisci and four principal ligaments—anterior/posterior cruciate ligaments (ACL/PCL) and lateral/medial collateral ligaments (LCL/MCL). Menisci were extensively meshed to allow for implementation of the circumferential orientation, the dominant collagen fiber directions. The prevailing meshes of tibial and femoral articular

cartilages (Dhaher et al. 2010) were extensively refined. Local coordinate systems were created to allow for realistic spatial representation of the collagen networks and solid matrix with depth-dependent variation in properties. In the superficial zone of the cartilage, the collagen fibrils are oriented horizontally parallel to the medial/lateral and anterior/posterior directions. In the transitional zone, the collagen fibrils are random (i.e., without any dominant orientations), following a gradual curvature that begins parallel to the superficial zone and turns perpendicular to the surface. In the deep zone, the vertical fibrils are oriented normal to the subchondral junction (Fig. 1). A value of 0.001 g/mm^3 was assigned for the density of all the soft tissues,(Penrose et al. 2002), whereas the bony structures were assigned with a density of 0.002 g/mm^3 (Hoffer 1983).

2.2 Material properties

2.2.1 Ligament

A transversely isotropic hyperelastic material model was considered for the major ligaments included in our model. The material model was assumed to be nearly incompressible (Dhaher et al. 2010) and was formulated using an uncoupled representation of the strain energy function defined by Limbert and Middleton (2004). In this framework, the fibers were assumed to be extensible and uniformly distributed in the ground substance, perfectly bonded to the matrix. The matrix was assumed to be isotropic and hyperelastic. With the proposed strain energy function, the exponential form of the classical nonlinear stiffening behavior of the collagen fibers under tension is achieved, and the collagen fibers are assumed not to support any compressive loads. Optimum set of material parameters characterizing the ligament model were obtained

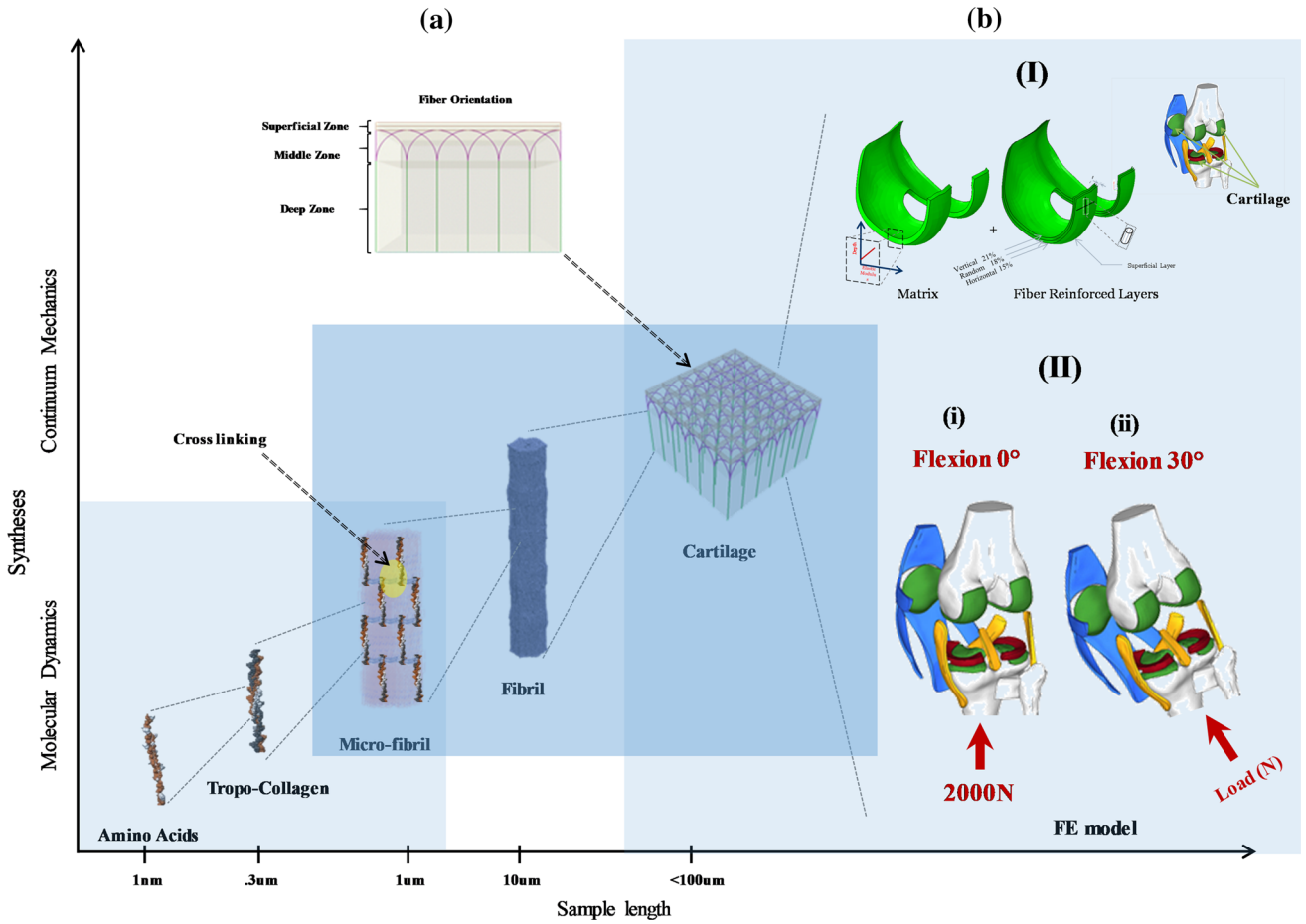

Fig. 1 (a) Schematic diagram showing the hierarchical features of the articular cartilage and orientation of the collagen fibrils as function of the depth. (b) (I) tibiofemoral joint finite element model used to simulate (II) (i) tibiofemoral joint axial compression under 2000 N axial load at full extension (ii) flexed tibia to 30° relative to the fixed femur and then axial loading applied parallel to the tibial axis until the initiation of the damage (fibril post-yield stretch). Damage initiation and its distribution were detected when the parameter (λ_{fp}) becomes greater than unity

from an extensive sensitivity and validation study (Dhaher et al. 2010) (Supplementary Materials).

2.2.2 Meniscus

The material characteristics of the meniscus are known to be inhomogeneous and anisotropic, but large variations in material property have been reported in the literature (Fithian et al. 1990; Lechner et al. 2000; Tissakht and Ahmed 1995). In the meniscal structure, the collagen fibers are arranged mainly in the circumferential direction (Aspden et al. 1985). These fibers supporting the large hoop stresses play an important role in the distribution of pressures within the tibiofemoral joint. It has been well documented that the modulus in the transverse and axial directions is approximately five to ten times less than that of the circumferential direction (Fithian et al. 1990; Proctor et al. 1989; Tissakht and Ahmed 1995) (see Supplementary Materials section Fig. 3). Therefore, to capture this anisotropic behavior, a transversely isotropic constitutive relationship was used for the meniscus (Donahue et al. 2003). This representation requires five independent parameters: circumferential modulus (E_C); transverse and axial modulus ($E_t = E_a$); shear modulus $G_t = G_a$, which describes the in-plane shear along the fiber direction; and Poisson's ratios. The first Poisson's ratio ($\nu_{ct} = \nu_{ca}$) defines the ratio of the contractile strain in the transverse plane to the tensile strain in the circumferential direction under circumferential load. The second Poisson's ratio (ν_{ta}) is defined within the transverse plane. Based on prior experimental studies, the circumferential modulus (E_C) was set to 120 MPa, and both the axial and transverse moduli ($E_T = E_a$) were assumed identical and were set to 20 MPa. The shear modulus was set to 47 MPa. The Poisson's ratios ($\nu_{ct} = \nu_{ca}$ and ν_{ta}) were set to 0.3, 0.45, respectively (Donahue et al. 2004; Skaggs et al. 1994; Tissakht and Ahmed 1995; Yao et al. 2006).

2.2.3 Cartilage

The fibril-reinforced composite model of the cartilage was developed by employing the multiplicative decomposition of the deformation gradients, an elastic and plastic part. To do so, the total deformation gradient tensor is given by $F = F_e F_p$, where e and p represent elastic and plastic components. The proposed hyper-elasto-plastic composite material model starts at the molecular level (tropocollagen, 300 nm) and extends to the macro-level (continua, > 100 µm). It is assumed that plastic flow of soft tissues is associated only with the uniaxial deformation of the collagen fibril (Tang et al. 2009). Neo-Hookean generalized strain energy is used to model the microfibril behavior as follows:

$$\psi_{\mathrm{fl}}\left(\bar{I}_{1\mathrm{e}}, \bar{I}_{4\mathrm{e}}\right) = \frac{1}{2}\mu^{\mathrm{fl}}\left(\bar{I}_{4\mathrm{e}}\right)\left(\bar{I}_{1\mathrm{e}} - 3\right) \tag{1}$$

where $\bar{I}_{1\mathrm{e}} = tr\,(\bar{C}_{\mathrm{e}} = \bar{F}_{\mathrm{e}}\,\bar{F}_{\mathrm{e}}^{\mathrm{T}})$ and $\bar{I}_{4\mathrm{e}} = n_0\,\bar{C}_{\mathrm{e}}\,n_0^t$ with n_0 being the microfibril reference direction at the initial configuration. The shear modulus μ_{fl} is considered as function of the elastic microfibril deformation with

$$\mu^{\mathrm{fl}}\left(\bar{I}_{4\mathrm{e}}\right) = \mu_0\left(\tanh\left(a_1\left(\bar{I}_{4\mathrm{e}} - 1\right)\right) - a_2\exp\left(a_3\left(\bar{I}_{4\mathrm{e}} - I_0\right)\right)\right) \tag{2}$$

where μ_0, a_i *and* I_0 represent the shear modulus, dimensionless parameters and the secondary stiffening of the microfibril, respectively. This hyperbolic function was used to fit the stiffness evolution of the microfibril predicted by molecular dynamic simulation during molecular dynamic analyses (Tang et al. 2009). The plastic flow in the microfibril was driven by the effective stress as follows:

$$\sigma_{\mathrm{eff}} = M : \mathrm{dev}\left(n_0 \otimes n_0\right) \tag{3}$$

where M is the Mandel stress

$$M = F^{\mathrm{eT}}\tau F^{\mathrm{e}\,-T} = F^{\mathrm{eT}}\left(2I_{4\mathrm{e}}\frac{\partial\psi_{\mathrm{fl}}}{\partial I_{4\mathrm{e}}}n_{\mathrm{e}} \otimes n_{\mathrm{e}}\right)F^{\mathrm{e}\,-T} \tag{4}$$

where τ and n_e stand for the macroscopic Kirchhoff stress and the microfibril current direction, respectively. By combining Eqs. (3) and (4), it can be readily shown that the effective stress takes the form

$$\sigma_{\mathrm{eff}} = \frac{4}{3}I_{4\mathrm{e}}\frac{\partial\psi_{\mathrm{fl}}}{\partial I_{4\mathrm{e}}} \tag{5}$$

The flow resistance is given by the following equation (Gasser and Holzapfel 2002; Tang et al. 2009):

$$\dot{g} = h\dot{\gamma}\left(1 - \frac{g}{g_{\mathrm{s}}}\right) \tag{6}$$

where g, g_{s} and h are the yield strength, saturated flow strength and hardening or softening rate, of the microfibril, respectively. Due to fibril softening associated with the breakage of cross-links, the saturated flow strength, g_s, is usually chosen to be lower than the initial yield strength of the microfibril (g_0) (Tang et al. 2009). This initial value is a function of the cross-link density between tropocollagen molecules (β) and is defined here by the density function as follows:

$$g_0 = g_i + c\beta^2 \tag{7}$$

$g_i\,(g_i = 400\,\mathrm{MPa})$ is the yield strength of the microfibril without cross-link, and c ($c = 11$) is a material constant (Tang et al. 2009). Coarse-graining procedure was employed to link the nanoscale collagen features and the tissue-level material properties, using the cross-link density function as a building block (Buehler 2006, 2008; Tang et al. 2009). By resolving the equation of equality between the effective stress and the yield strength of the microfibril (g), a critical value $\bar{I}_{\mathrm{cr}}$ can be determined such that the yielding occurs when $\bar{I}_4 = \bar{I}_{\mathrm{cr}}$.

Thereafter, the evolution of the plastic strain in the fibril is driven by the single-crystal plasticity model (Belytschko et al. 2014; Gasser and Holzapfel 2002; Tang et al. 2009):

$$\dot{\gamma} = \dot{\gamma}_0 \left| \frac{\sigma_{\text{eff}}}{g} \right|^{1/m} \text{sig}\left(\sigma_{\text{eff}}\right) \tag{8}$$

where $\dot{\gamma}$ is the plastic strain rate and g is the yield strength of the microfibril. Here, the system is assumed to obey the following (Karush–Kuhn–Tucker) loading/unloading conditions:

$$\dot{\gamma} \geq 0; \quad f = (\sigma_{\text{eff}} - g) \leq 0; \quad f\dot{\gamma} = 0 \tag{9}$$

Once the plastic strain rate was calculated, the plastic deformation tensor was updated based on integration of the plastic velocity gradient equation (Gasser and Holzapfel 2002):

$$\dot{F}_{\text{p}} = \dot{\gamma}\, \text{dev}\left(n_0 \otimes n_0\right) F_{\text{p}} \tag{10}$$

Then, the elastic gradient tensor of deformation was updated using the deformation gradient decomposition equation as follows:

$$F_{\text{e}} = F F_{\text{P}}^{-1} \tag{11}$$

And the fibrils plastic stretch is calculated from the basic definition of stretch

$$\lambda_{\text{fp}} = \sqrt{\bar{I}_{4\text{p}}} \tag{12}$$

The λ_{fp} is assumed to be unity during the elastic phase of the response ($F_{\text{p}} = I$ and $F_{\text{e}} = F$). Then, the yield initiation and its distribution were detected when the parameter (λ_{fp}) becomes greater than unity. Based on the microfibril behavior, generalized neo-Hookean strain energy function is used to model the fibril and tissue behavior by considering the rule of mixtures (for more details, please see Supplementary Materials section).

The volume fractions of collagen fibril in cartilage were assumed to be 15%, 18% and 21% in the superficial, transitional and deep zones, respectively (Shirazi et al. 2008). To reflect the incompressibility of the articular cartilage during the transient (short-term) biphasic response, an equivalent elastic response was sought by using the equilibrium (drained) modulus of the tissue with a Poisson's ratio of 0.5. The drained modulus was considered to be depth dependent varying from 0.3 to 1.2 MPa, descending from the cartilage surface to lowermost layer at the subchondral bone interface (Schinagl et al. 1997). The shear moduli of the fibril matrix and microfibril were 2.879 MPa and 2906.928 MPa, respectively. The volume fraction of microfibril and secondary stiffness were 0.212 and 2.118, respectively. The cross-link density between the tropocollagen molecules (β) was 9 ($g_0 = 1291$ MPa) with 0.01 and 0.05 as initial plastic strain rate and rate sensitivity, respectively. Details on the materials formulation and the considered parameters and their values, model validation and verification can be found in Supplementary Materials and prior work (Adouni and Dhaher 2016).

2.3 Loading and boundary conditions

To test the viability of a multiscale model of the cartilaginous tissue coupled with the FE model of the healthy joint, axial compression loading condition was simulated. The compression force was applied with the tibiofemoral joint at full extension and at a flexed posture. For both loading conditions, the femur was fixed. The tibial degrees of freedom were unconstrained except for the tibial flexion angle. Simulation outputs include cartilage loading/damage, represented by the sub(elastic)- and post-(plastic)-yielding states. For the sub-yielding state (elastic), the tibiofemoral joint passive response (compression force vs. axial displacement) was investigated at full extension under 2000 N of axial compressive load. To facilitate the comparison to the few experimental data on average and peak contact pressure reported in the literature (pre-yield) (Ahmed and Burke 1983; Brown and Shaw 1984; Poh et al. 2012; Seitz et al. 2012), simulations were conducted for a range of compression forces (200 to 2000 N).

In an attempt to qualitatively verify our predictions of the post-yield response, we compared our simulation results to the singular joint-level experimental data reported in the literature. Meyer et al. (2008) reported cartilage damage patterns and the associated load threshold in cadaveric knee specimens. With the tibia flexed at 30°, axial loads parallel to the tibial axis were applied until the damage was initiated. Hence, model simulations were conducted to emulate these experimental boundary conditions (fully constrained femur, 30° tibial flexion, fixed tibial varus/valgus rotation and 7000 N axial load applied on the tibial bone). The output of the simulations included model-predicted cartilage failure patterns (fibril post-yield stretch distribution) and the associated damage inducing axial load. To test the sensitivity of the predicted results as a function of the cross-link density between the tropocollagen molecules (β), simulations were repeated by varying the value of β from 8 to 14. Abaqus explicit was used during all simulations with a short step time of 0.01 s to mimic quasi-static analysis (for details, see Supplementary Materials).

3 Results

Figure 2 depicts the nonlinear trend of axial displacement of the tibiofemoral joint subjected to tibial compression force varying from 0 to 2000 N, with a 1.69 mm of maximum

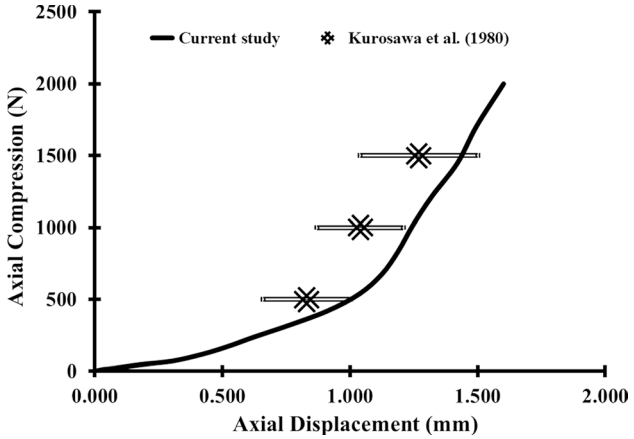

Fig. 2 Tibial axial translation under compressive load up to 2000 N. Experimental measurements under the same boundary conditions also shown for comparison. (Kurosawa et al. 1980)

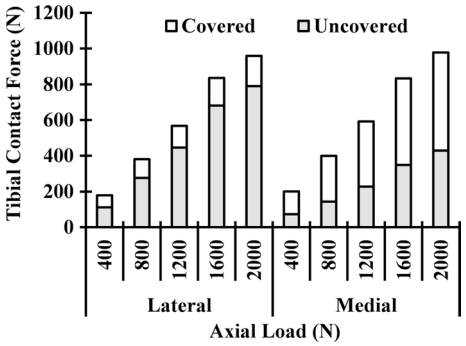

Fig. 3 Predicted compartmental axial contact force at covered (menisci–cartilage) and uncovered (cartilage–cartilage) areas during axial load of 2000 N

displacement observed at the 2000 N force level. In response to the axial compression (2000 N), 1.5 and 3.4 mm of lateral and anterior tibial displacements were observed, respectively. A relatively small valgus rotation (0.9°) and a much greater internal rotation (~6°) have also been computed.

Across all loading conditions, the contact force levels at the medial and lateral tibial plateaus were comparable (Fig. 3) with a maximum difference less than 40 N. On the lateral plateau, ~85% of the contact was supported by the uncovered zone (cartilage–cartilage contact), and only 50% of the load has been transmitted through the uncovered area of the medial plateau (Fig. 3). The total contact area across the tibiofemoral joint increased from 360 mm^2 at no load to 1301 mm^2 when an axial tibial load of 2000 N was applied. By varying the axial load from 1000 to 2000 N, the average contact pressure on the tibial plateau nearly doubled from 0.79 to 1.64 MPa. As shown in Fig. 4, the tibial contact pressure reached a maximum of ~4 MPa on the lateral plateau at 2000 N axial force. Apart from the central loading zone, both randomly oriented and vertical fibrils (at the middle and deep zones, respectively) have been subjected to large stress and strain (Fig. 5). The maximum stresses were 6.24 MPa, 2 MPa and 5.19 MPa at the superficial, middle and bottom layers of the articular cartilage, all expressed in the lateral plateau, respectively (for details, see Supplementary Materials).

At 30° tibiofemoral joint flexion and with a cross-link density of 9 (the calibrated value of β as reported by Adouni and Dhaher (2016)), model prediction indicates that cartilage damage was initiated with 4960 N of compression force with 29 MPa maximum contact pressure on the lateral plateau (Fig. 6). Mises stresses were much larger in the superficial layer and reached a maximum of

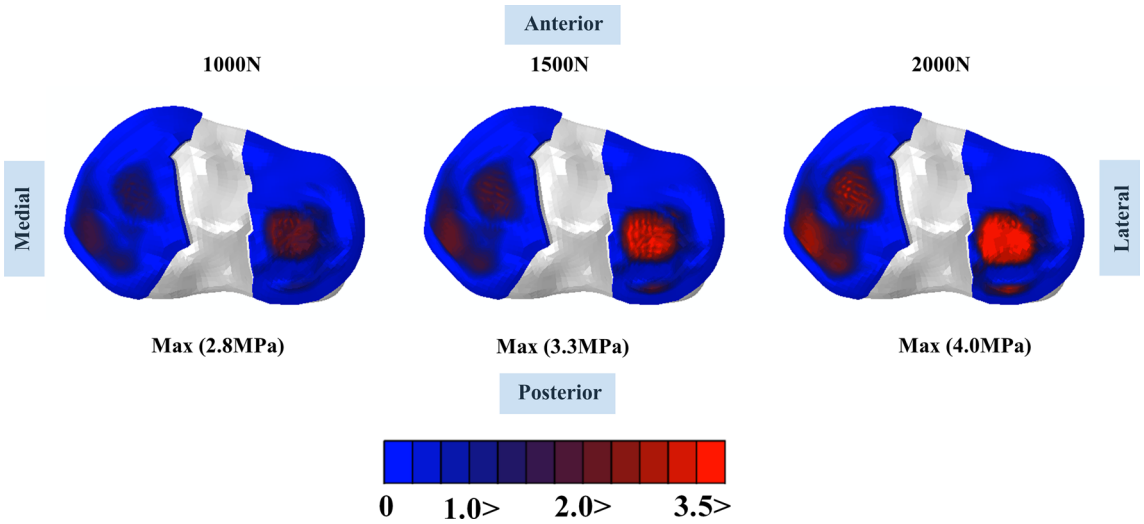

Fig. 4 Predicted contact stress on the tibial cartilage under 1000 N, 1500 N and 2000 N axial load

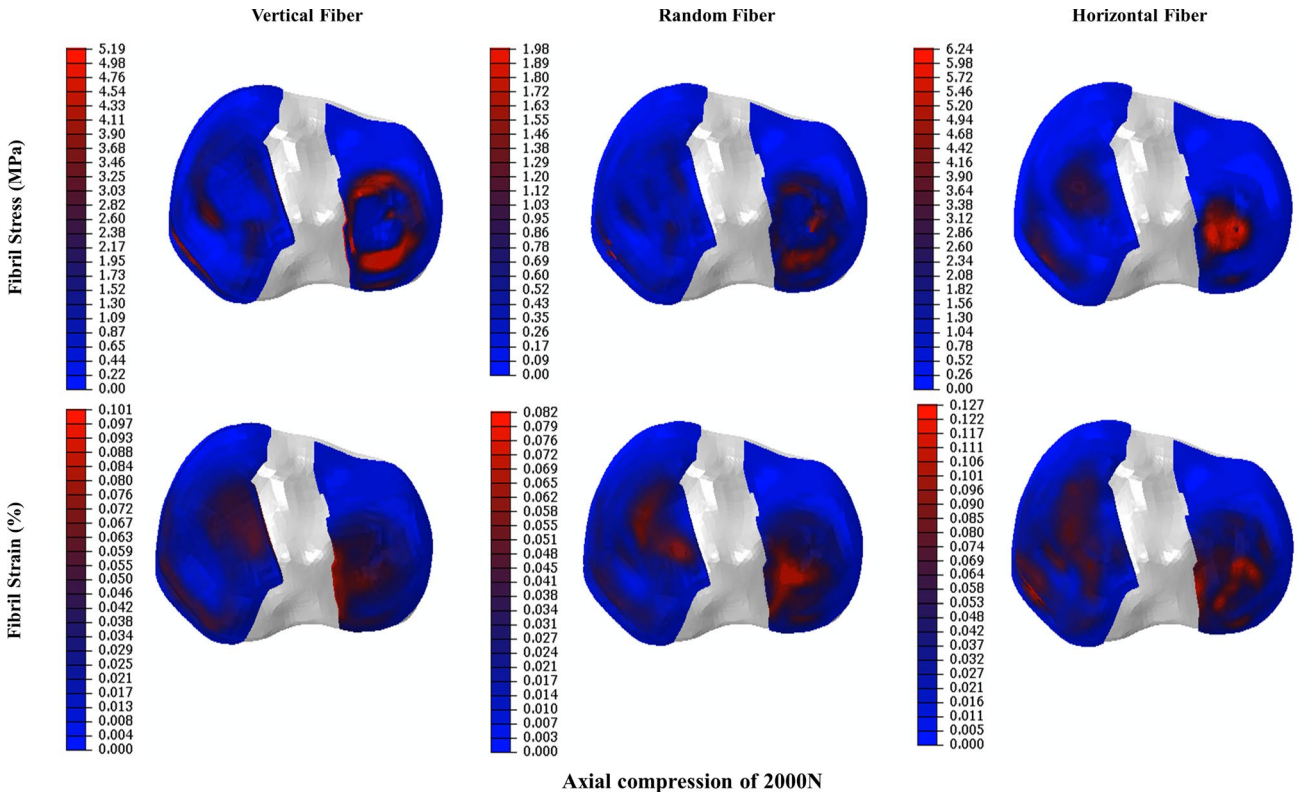

Fig. 5 Predicted max fibrils stress/strains on the three different layers of the tibial article cartilage under 2000 N axial compression. The presented distributions are for the surface and transitional zones between the different layers of the articular cartilage

31 MPa at 28% fibrils axial strain. Slightly higher values were computed for the femoral cartilage fibrils (~7%). A clear correlation has been observed between the fibrils level metric of damage (λ_{fp}) (axial fibril plastic stretch) and the tibiofemoral joint average contact pressure (positive $r=0.98$ (anterior–posterior) $r=0.99$ (medial–lateral)) and maximal Mises stress (negative $r=-0.97$) (Figs. 7 and 8b). Figure 8 shows the load required to initiate cartilage fibril damage increased by 2881 N when the cross-link density (β) changed from 8 to 14. Here, the yield strength of articular cartilage also increases with the increasing cross-link density. Model predictions indicated that the damage distribution (fibril post-yield stretch distribution) to the articular fibril network was limited to the superficial and middle zones. This damage distribution has been expressed in the lateral compartment starting, in all cross-link density states, from the area near the PCL foot print, where λ_{fp} reaches a maximum of 1.394. The area of cartilage damage decreased substantially from 194 to 21 mm^2 with cross-link density (β), varying from 8 to 14, respectively (Fig. 8). Similar distribution was observed on the femoral side (data not shown); however, the damage was limited to the superficial layer for the boundary conditions used in this study.

4 Discussion

In the present work, we studied the mechanical response and failure mechanisms of a multiscale, three-layered hierarchical cartilage model embedded in a high-fidelity FE model of the human tibiofemoral joint under quasi-static compressive loading. The high-fidelity model accounted for the joint passive properties and computed the stress/strain at the tissue level as a function of molecular properties at the tropocollagen level. The loading conditions used corresponded to levels seen during normal activities of daily living. Simulation results of the pre-yield behavior were consistent with experimental data reported on the aggregate joint kinematics and cartilage contact properties under similar loading conditions. Our findings also indicated that the aggregate stress distribution within a given layer in the cartilage does not serve as predictor of failure sites, defined herein at the tropocollagen level. Indeed, while the minimum value of the aggregate maximum stress across the three cartilage layers was located in the middle layer, failure was computationally detected in both the superficial and middle layers but not in the bottom layer with a significantly higher maximum stress. The

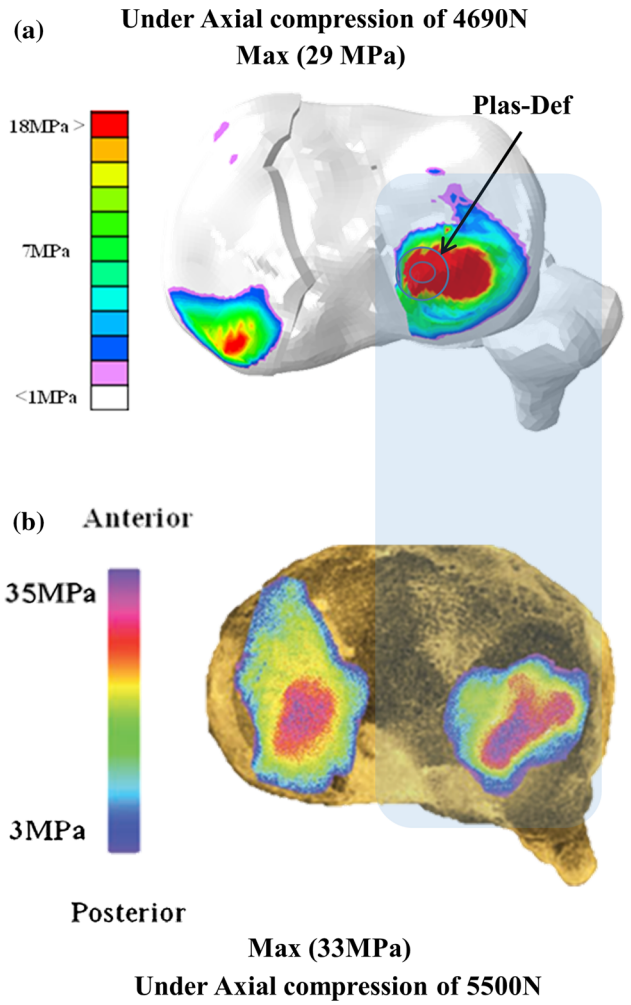

Fig. 6 **a** FE prediction along with **b** measured contact pressure of cartilage at failure (Meyer et al. 2008) during high axial loading when the joint flexed by 30°

results from this study show that cartilage surface failure can form purely by mechanical means, and this failure is cross-link density dependent. In this context, our simulation results indicate that increased tropocollagen cross-link density improved the pre-yield load-bearing capacity of the cartilage. Our simulation results also indicated that that the stiffer the fibril is (higher cross-link densities, β), the higher the contact stress required to elicit a fibril yield and the higher the rate of yielding as a function of increased contact stress. These findings suggest that induced acute cartilage damage is dependent on the highly sensitive relationship between aggregate joint loading and cartilage micromechanics at the tropocollagen level.

We sought to examine whether the inclusion of the complex cartilage model and the corresponding mechanics affects the predicted aggregate joint behavior. In this context, we cross-examined the joint-level kinematics and kinetics against reported cadaveric data obtained under similar boundary conditions. The simulated axial deflection agreed with the measurement performed under axial displacement with similar boundary conditions. Experimental compression tests (load levels, 1500 N) reported axial displacements of 1.27 mm with unconstrained secondary rotations, (Kurosawa et al. 1980) a value consistent with the model-predicted axial displacement (1.46 mm). Analogous trend and values were also observed on the rest of degrees of freedom (frontal and sagittal) of the tibial bone when the model predictions were compared to experimental reports (Allaire et al. 2008). Our model simulations also indicated that the relative load contribution on the meniscus in both compartments decreased with compression force, an observation consistent with reported experimental and numerical data (Ahmed and Burke 1983; Bendjaballah et al. 1995; Shirazi et al. 2008; Walker and Erkman 1975). The maximal (4 MPa) and average (1.34 MPa) contact pressures in response to the 2000 N axial load were estimated and were within the experimentally reported values under similar loading conditions (Inaba et al. 1990; Poh et al. 2012). Our model predictions also indicated that ACL force increased with increasing compression force, reaching a maximum value of 96 N at 2000 N compression force. Markolf et al.(2014) reported a resultant ACL force of 56 ± 20 N under 500 N axial compression. The model-predicted value under the same loading conditions was 33 N. While the currently predicted ACL force was with the experimental range, a greater ACL force (163 N) was predicted by Shirazi et al.(2008). The difference in the estimate may be in part due to the difference in the material properties used for the connective tissues and the difference in the geometry of the two models (Marouane et al. 2015). The small displacement on the lateral side results in a low (less than 20 N) equally distributed force between the collateral ligaments (MCL and LCL) with an unloaded PCL over the range of compression forces used in the simulations. This phenomenon is consistent with earlier predictions and measurements (Markolf et al. 1981; Shirazi et al. 2008). Taken together, our compression/deflection, contact stress and connective tissue force predictions support the viability of the proposed model in predicting the aggregate mechanics of the tibiofemoral joint under physiological loading in the sub-yielding state (see data in Supplementary Materials under the additional results subsection).

The pre-yield maximum peak stresses estimated in this study ranged from 2.8 to 4.0 MPa depending on the compression force levels, within the range of peak stresses acting on cartilage during light to moderate activities (Ahmed and Burke 1983). Our simulation results indicated that the maximum stress and strain were expressed in the superficial layer, where the collagen fibrils are oriented perpendicular to the loading direction (Fig. 5). This observation may be due in part to the horizontal expansion of the articular cartilage experiences during the axial compression of the tibiofemoral

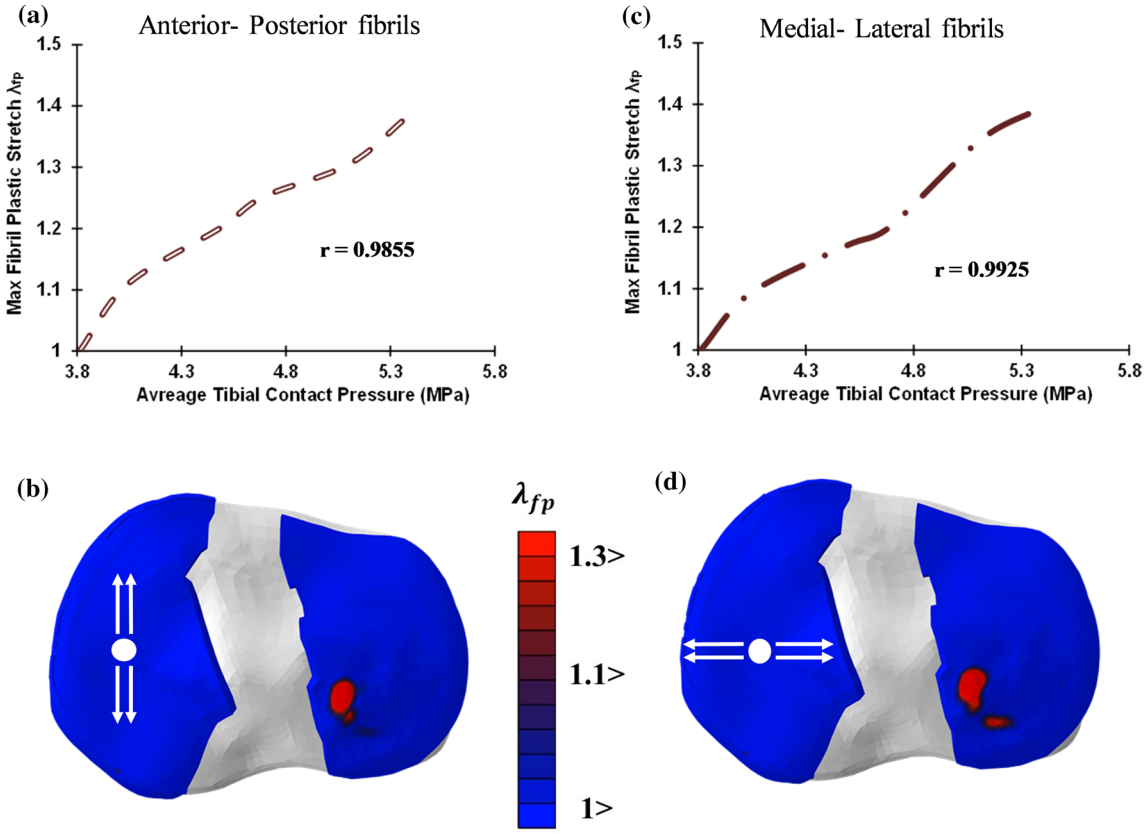

Fig. 7 Cartilage fibril post-yield stretch (damage) when the joint is flexed by 30°, **a**, **c** maximum fibril plastic stretch λ_{fp} as function of average tibial contact pressure in the anterior–posterior and medial–lateral fibrils directions (with a correlation coefficients $r=0.9855$ (anterior–posterior) and $r=0.9925$ (medial–lateral)), **b**, **d** fibril post-yield stretch distribution on the anterior–posterior and medial–lateral fibrils directions (this distribution is the area where the collagen fibrils exhibited a post-yield state)

joint. In contrast, no load has been supported by the vertical fibrils immediately underneath the loading center, an observation reported by prior numerical and experimental examinations (Kaab et al. 1998; Shirazi and Shirazi-Adl 2005). For the bottom layer, fibrils in the circumference of the circular stress pattern shown in Fig. 5 were in tension while collagen fibrils at the center of the pattern were under compression. In addition, the maximum tension in the bottom layer fibrils was estimated at the osteochondral junction. A large amount of fibril stress/strain in both the superficial (5.4 MPa/7.4%) and deep layers (4.2 MPa/6.2%) of the articular cartilage was also observed in our previous axisymmetric specimen model under indentation test of 12% axial displacement (Adouni and Dhaher 2016). However, when employed in the full 3D tibiofemoral model, our multiscale, three-layered model of the cartilage indicated that the stress concentration on the fibrils was expressed in the anterior–posterior directions. This prediction may be due to the oval-like area between the femoral and tibial cartilages.

One of the key barriers to examinations similar to the current study is the lack of experimental data identifying load thresholds of tibial cartilage failure in a full joint model. In a singular study, Meyer et al. (2008) identified the failure patterns in the tibial cartilage under axial loading. By flexing the tibiofemoral joint to 30° and applying a high axial load on the tibial axis, the micro-cartilage damage was observed on the superficial and deep layers of the lateral plateau. In their report, the damage started approximately at 5500 N (±2000 N) with a 33 MPa (±9 MPa) peak contact stress. Our multiscale, multilayered model predictions indicated that cartilage failure was achieved when a 4960 N compression force was applied with a corresponding cartilage stress of 29 MPa (Fig. 6). The model-predicted location of the "cartilage damage" was qualitatively similar to the observed locations reported by the aforementioned experiment (Meyer et al. 2008). However, cartilage stress distribution on the medial plateau was more posteriorly located compared with the Meyer measurements. This may be explained by the observed external rotation of the tibiofemoral joint that was associated with posterior translation during knee flexion and under high axial tibial load. The study by Meyer and colleagues did not identify the failure initiation process in the context of the different layers of the cartilage. However, from the few experimental paradigms on the patellofemoral

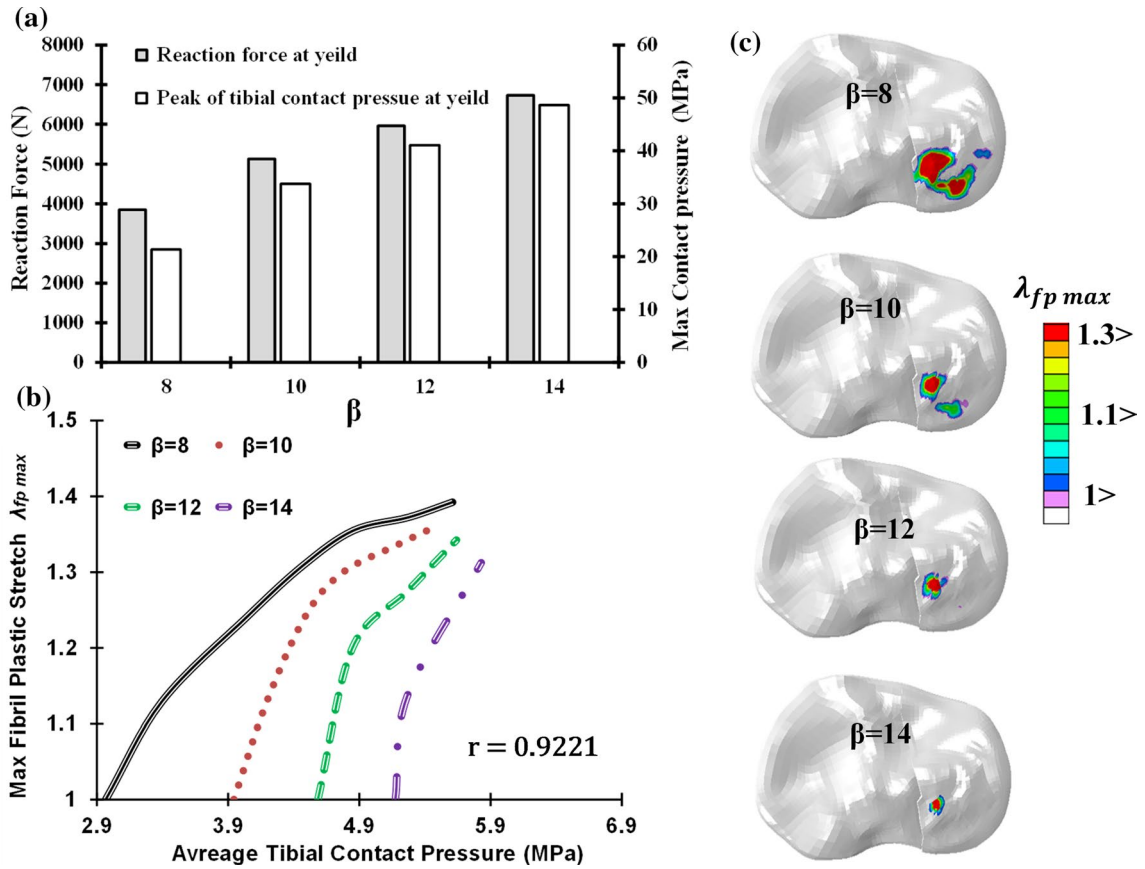

Fig. 8 **a** Predicted contact stress and reaction forces (axial load at the joint) at fibril yield, **b** the maximum fibril plastic stretch λ_{fpmax} (maximum value stretch of the two fibril bundles (anterior–posterior and medial–lateral) defined as $\lambda_{\mathrm{fpmax}} = \max\left\{\lambda_{\mathrm{fp(ant-post)}};\lambda_{\mathrm{fp(med-lat)}}\right\}$) as function of average tibial contact pressure post-yield (with an average of correlation coefficient $r = 0.9221$) and **c** propagation of cartilage fibril post-yield stretch distribution (damage) under varied cross-link densities (β) when the joint flexed by 30°

joint damage, in addition to the superficial layer fibrillation, micro-cracks at the osteochondral junction in the lowermost area of the articular cartilage were reported (Armstrong et al. 1985; Atkinson and Haut 1995). It has been postulated that this failure is due to the excessive shear stress at the interface between the hyaline and the calcified layers of the cartilage. While the association between the superficial layer fibrillation and bottom layer cracking has been proposed, data on damage initiation in the cartilage are lacking. In our model, collagen damage distribution (fibril post-yield stretch distribution) started at the anterior–posterior direction and then propagated into the medial–lateral direction of the fibrils in the superficial layer. The damage eventually is expressed in the upper layer of the mid-region where the collagen fibrils are randomly oriented. These findings suggest that reports on cartilage failure originated in the surface layer of the cartilage. The model proposed here can be used to viably examine failure properties that are experimentally difficult to delineate, such as cartilage damage initiation, propagation and distribution. Identifying these properties may inform current interest in biological repair and resurfacing of the cartilage defects: for example, lavage and shaving arthroscopic interventions, mainly superficial treatment of cartilage, characterized by 50% of success among the treated population. This low success rate may be due in part to the simultaneous presence of micro-cracks of the lowermost layers of the articular cartilage that were not directly managed (Brittberg and Winalski 2003; Hunziker 2002; Sgaglione 2003; Tyyni and Karlsson 2000).

Change in contact pressure has often been employed as an indirect tool to evaluate the severity of certain loading conditions experienced by the knee joint (Adouni and Shirazi-Adl 2009; Besier et al. 2005; Farrokhi et al. 2011; Guess et al. 2013; Halonen et al. 2017; Ho et al. 2014; Mokhtarzadeh et al. 2013; Shirazi and Shirazi-Adl 2009). In these examinations, modelers either directly or indirectly interpret their estimates of cartilage average contact stress to the "health" of the cartilage by comparing to experimental data—an "observable damage" of the cartilage—defining the threshold for adverse joint loading. Hence, these studies used the average contact pressure as a proxy variable to cartilage damage, for the most part, to be consistent with

experimentally reported quantities (Brand 2005; Danso et al. 2014; Kaukinen et al. 2005; Mononen et al. 2016). However, prior to the observed damage of the cartilage, measurement of the micro-damage initiated at the tissue level in a cadaveric joint model under a given loading condition is difficult. Our data illustrated in Figs. 7 a, c and 8b can be considered as a mapping between an aggregate contact property and micro-damage at the fibril level, a mapping that cannot be obtained experimentally and can be used to more accurately define loading of the joint that will yield "damage" in its multiscale expression.

The proposed multiscale, multilayered hierarchical model of the cartilage used in the 3D model of the tibiofemoral joint is a generalization of the calibrated and validated specimen-based model of the cartilage previously published (Adouni and Dhaher 2016). In this generalization, two fibrils orientations were proposed for the superficial layer. The two dominant directions—medial/lateral and anterior/posterior—adopted here were based on the earlier observation indicating a minimal effect of this assumption on the contact parameter during knee modeling (Mononen et al. 2012). While the localized properties of the articular may affect the predicted initiation and propagation of the fibril damage, the predicted location of the damage is consistent with the softening area on the cartilage observed in a recent in vitro study (Deneweth et al. 2013). To facilitate comparison to existing data, we exposed the model to different boundary conditions synonymous with those used in the reported experimental data (elastic and plastic responses of the tissue). In addition, the plastic response of the cartilage model was associated only with the uniaxial deformation of the collagen fibril and not considered for the rest of the components of the articular cartilage matrix. It is noteworthy to state that the current results and conclusions are restricted to short-term cartilage as well as meniscal responses. While the meniscus is characterized by high inhomogeneity with a fiber-reinforced nonlinear mechanical behavior that depends on the mode of loading (tensile or compressive), in this model we assumed a homogenous and transversely isotropic elastic behavior of the tissue. This transversely isotropic constitutive relationship was well documented to capture the anisotropic behavior of the meniscus under compressive loading (Donahue et al. 2003). It remains to be seen if our estimation of the cartilage fibril elasto-plastic behavior is influenced by the lack of inclusion of the inhomogeneity and tensile mechanics of the meniscus.

5 Conclusions

We studied the mechanical response and failure mechanisms of a multiscale, three-layered cartilage model embedded in a high-fidelity finite element model of the human tibiofemoral joint under a quasi-static compressive loading. The high-fidelity model accounted for the joint passive properties and computed the stress/strain at the tissue level as a function of molecular properties at the tropocollagen level. To the best of our knowledge, this is the first model that simultaneously predicted the macro-continuum joint mechanics as the function of the micro-level characteristics of the tissue. We argue that results gleaned from this study provide important insights to our understanding of the etiology of cartilage and joint damage. Linking the micro- to the macro-behaviors will also help future examination on the connection between aging/diabetes-mediated changes in cross-link density and the aggregate cartilage and joint mechanics (Gautieri et al. 2014).

Acknowledgements This work is supported by a Grant (#U01 EB015410-01A1) from the National Institute of Health NIH.

Authors' contribution All authors have read and approved this submission; M.A. carried out analyses, all (M.A., T.F., M.G. and Y.D.) participated in the definition, design and development of the work, and finally manuscript was written by all authors (M.A., T.F., M.G. and Y.D.).

Compliance with ethical standards

Conflict of interest There is no conflict of interest to declare.

References

Abrahams M (1967) Mechanical behaviour of tendon in vitro. Med Biological Eng 5:433–443

Abusara Z, Seerattan R, Leumann A, Thompson R, Herzog W (2011) A novel method for determining articular cartilage chondrocyte mechanics in vivo. J Biomech 44:930–934

Adouni M, Dhaher YY (2016) A multi-scale elasto-plastic model of articular cartilage. J Biomech 49:2891–2898

Adouni M, Shirazi-Adl A (2009) Knee joint biomechanics in closed-kinetic-chain exercises. Comput Methods Biomech Biomed Eng 12:661–670

Adouni M, Shirazi-Adl A, Shirazi R (2012) Computational biodynamics of human knee joint in gait: from muscle forces to cartilage stresses. J Biomech 45:2149–2156

Ahmed A, Burke D (1983) In-vitro of measurement of static pressure distribution in synovial joints—part I: tibial surface of the knee. J Biomech Eng 105:216

Allaire R, Muriuki M, Gilbertson L, Harner CD (2008) Biomechanical consequences of a tear of the posterior root of the medial meniscus: similar to total meniscectomy. JBJS 90:1922–1931

Armstrong CG, Mow VC, Wirth CR (1985) Biomechanics of impact-induccd microdamage to articular cartilage: a possible genesis for chondromalacia patella. Paper presented at the symposium on sports medicine, St. Louis USA, 1985

Aspden R, Yarker Y, Hukins D (1985) Collagen orientations in the meniscus of the knee joint. J Anat 140:371

Astephen JL (2007) Biomechanical factors in the progression of knee osteoarthritis. Ph.D., Dalhousie University

Atkinson PJ, Haut RC (1995) Subfracture insult to the human cadaver patellofemoral joint produces occult injury. J Orthop Res 13:936–944

Bank RA, Soudry M, Maroudas A, Mizrahi J, TeKoppele JM (2000) The increased swelling and instantaneous deformation of osteoarthritic cartilage is highly correlated with collagen degradation. Arthritis Rheum 43:2202–2210

Barbour KE, Helmick CG, Boring M, Brady TJ (2017) Vital signs: prevalence of doctor-diagnosed arthritis and arthritis-attributable activity limitation-United States, 2013–2015. MMWR Morb Mortal Wkly Rep 66:246–253

Belytschko T, Liu WK, Moran B, Elkhodary K (2014) Nonlinear finite elements for continua and structures. Wiley, Hoboken

Bendjaballah M, Shirazi-Adl A, Zukor D (1995) Biomechanics of the human knee joint in compression: reconstruction, mesh generation and finite element analysis. Knee 2:69–79

Besier TF, Gold GE, Beaupré GS, Delp SL (2005) A modeling framework to estimate patellofemoral joint cartilage stress in vivo. Med Sci Sports Exerc 37:1924–1930

Bi X, Li G, Doty SB, Camacho NP (2005) A novel method for determination of collagen orientation in cartilage by Fourier transform infrared imaging spectroscopy (FT-IRIS). Osteoarthr Cartil 13:1050–1058

Brand RA (2005) Joint contact stress: a reasonable surrogate for biological processes? Iowa Orthop J 25:82

Brittberg M, Winalski CS (2003) Evaluation of cartilage injuries and repair. JBJS 85:58–69

Brown TD, Shaw DT (1984) In vitro contact stress distribution on the femoral condyles. J Orthop Res 2:190–199

Buehler MJ (2006) Nature designs tough collagen: explaining the nanostructure of collagen fibrils. Proc Natl Acad Sci USA 103:12285–12290

Buehler MJ (2008) Nanomechanics of collagen fibrils under varying cross-link densities: atomistic and continuum studies. J Mech Behav Biomed Mater 1:59–67

Buehler MJ, Ballarini R (2013) Materiomics: multiscale mechanics of biological materials and structures. Springer, Berlin

Danso E, Honkanen J, Saarakkala S, Korhonen R (2014) Comparison of nonlinear mechanical properties of bovine articular cartilage and meniscus. J Biomech 47:200–206

Deneweth JM, Newman KE, Sylvia SM, McLean SG, Arruda EM (2013) Heterogeneity of tibial plateau cartilage in response to a physiological compressive strain rate. J Orthop Res 31:370–375

Dhaher YY, Kwon TH, Barry M (2010) The effect of connective tissue material uncertainties on knee joint mechanics under isolated loading conditions. J Biomech 43:3118–3125

Donahue TL, Hull ML, Rashid MM, Jacobs CR (2002) A finite element model of the human knee joint for the study of tibio-femoral contact. J Biomech Eng 124:273–280

Donahue TLH, Hull ML, Rashid MM, Jacobs CR (2003) How the stiffness of meniscal attachments and meniscal material properties affect tibio-femoral contact pressure computed using a validated finite element model of the human knee joint. J Biomech 36:19–34

Donahue TLH, Hull ML, Rashid MM, Jacobs CR (2004) The sensitivity of tibiofemoral contact pressure to the size and shape of the lateral and medial menisci. J Orthop Res 22:807–814

Farrokhi S, Keyak J, Powers C (2011) Individuals with patellofemoral pain exhibit greater patellofemoral joint stress: a finite element analysis study. Osteoarthr Cartil 19:287–294

Fithian DC, Kelly MA, Mow VC (1990) Material properties and structure–function relationships in the menisci. Clin Orthop Relat Res 252:19–31

Fratzl P (2008) Collagen: structure and mechanics. Springer, Berlin

Gasser TC, Holzapfel GA (2002) A rate-independent elastoplastic constitutive model for biological fiber-reinforced composites at finite strains: continuum basis, algorithmic formulation and finite element implementation. Comput Mech 29:340–360

Gautieri A, Redaelli A, Buehler MJ, Vesentini S (2014) Age- and diabetes-related nonenzymatic crosslinks in collagen fibrils: candidate amino acids involved in advanced glycation end-products. Matrix Biol 34:89–95

Guess TM, Liu H, Bhashyam S, Thiagarajan G (2013) A multibody knee model with discrete cartilage prediction of tibio-femoral contact mechanics. Comput Methods Biomech Biomed Eng 16:256–270

Halonen K, Dzialo CM, Mannisi M, Venäläinen M, Zee M, Andersen MS (2017) Workflow assessing the effect of gait alterations on stresses in the medial tibial cartilage-combined musculoskeletal modelling and finite element analysis. Sci Rep 7:17396

Ho K-Y, Keyak JH, Powers CM (2014) Comparison of patella bone strain between females with and without patellofemoral pain: a finite element analysis study. J Biomech 47:230–236

Hoffer MM (1983) A primer of orthopaedic biomechanics. JAMA 249:2397

Holzapfel GA, Gasser TC, Ogden RW (2000) A new constitutive framework for arterial wall mechanics and a comparative study of material models. J Elast Phys Sci Solids 61:1–48

Hunziker E (2002) Articular cartilage repair: basic science and clinical progress. A review of the current status and prospects. Osteoarthr Cartil 10:432–463

Inaba HI, Arai MA, Watanabe WW (1990) Influence of the varus–valgus instability on the contact of the femoro-tibial joint. Proc Inst Mech Eng H 204:61–64

Julkunen P, Wilson W, Jurvelin JS, Rieppo J, Qu C-J, Lammi MJ, Korhonen RK (2008a) Stress–relaxation of human patellar articular cartilage in unconfined compression: prediction of mechanical response by tissue composition and structure. J Biomech 41:1978–1986

Julkunen P, Wilson W, Jurvelin JS, Rieppo J, Qu CJ, Lammi MJ, Korhonen RK (2008b) Stress-relaxation of human patellar articular cartilage in unconfined compression: prediction of mechanical response by tissue composition and structure. J Biomech 41:1978–1986

Kaab MJ, Ito K, Clark JM, Notzli HP (1998) Deformation of articular cartilage collagen structure under static and cyclic loading. J Orthop Res 16:743–751

Kaukinen AP, Laasanen MS, Lammentausta E, Halmesmäki E, Helminen HJ, Jurvelin JS, Rieppo J (2005) Destructive testing of articular cartilage in compression—effect of collagen network. Paper presented at the 51st Annual Meeting of the Orthopaedic Research Society, Washington, DC, 2005

Kraus VB, Blanco FJ, Englund M, Karsdal MA, Lohmander LS (2015) Call for standardized definitions of osteoarthritis and risk stratification for clinical trials and clinical use. Osteoarthr Cartil 23:1233–1241

Kurosawa H, Fukubayashi T, Nakajima H (1980) Load-bearing mode of the knee-joint—physical behavior of the knee-joint with or without menisci. Clin Orthop Relat Res 149:283–290

Lechner K, Hull M, Howell S (2000) Is the circumferential tensile modulus within a human medial meniscus affected by the test sample location and cross-sectional area? J Orthop Res 18:945–951

Limbert G, Middleton J (2004) A transversely isotropic viscohyperelastic material—application to the modeling of biological soft connective tissues. Int J Solids Struct 41:4237–4260

Malaspina DC, Szleifer I, Dhaher Y (2017) Mechanical properties of a collagen fibril under simulated degradation. J Mech Behav Biomed Mater 75:549–557

Markolf KL, Bargar WL, Shoemaker SC, Amstutz HC (1981) The role of joint load in knee stability. J Bone Joint Surg Am 63:570–585

Markolf KL, Jackson SR, Foster B, McAllister DR (2014) ACL forces and knee kinematics produced by axial tibial compression during a passive flexion–extension cycle. J Orthop Res 32:89–95

Marouane H, Shirazi-Adl A, Adouni M (2015) Knee joint passive stiffness and moment in sagittal and frontal planes markedly

increase with compression. Comput Methods Biomech Biomed Eng 18:339–350
Maroudas A, Bullough P, Swanson S, Freeman M (1968) The permeability of articular cartilage. J Bone Jt Surg Br 50:166–177
Meyer EG, Baumer TG, Slade JM, Smith WE, Haut RC (2008) Tibiofemoral contact pressures and osteochondral microtrauma during anterior cruciate ligament rupture due to excessive compressive loading and internal torque of the human knee. Am J Sports Med 36:1966–1977
Mokhtarzadeh H, Yeow CH, Hong Goh JC, Oetomo D, Malekipour F, Lee PV (2013) Contributions of the soleus and gastrocnemius muscles to the anterior cruciate ligament loading during single-leg landing. J Biomech 46:1913–1920
Mononen ME, Julkunen P, Toyras J, Jurvelin JS, Kiviranta I, Korhonen RK (2011) Alterations in structure and properties of collagen network of osteoarthritic and repaired cartilage modify knee joint stresses. Biomech Model Mechanobiol 10:357–369
Mononen ME, Mikkola MT, Julkunen P, Ojala R, Nieminen MT, Jurvelin JS, Korhonen RK (2012) Effect of superficial collagen patterns and fibrillation of femoral articular cartilage on knee joint mechanics-a 3D finite element analysis. J Biomech 45:579–587
Mononen ME, Tanska P, Isaksson H, Korhonen RK (2016) A novel method to simulate the progression of collagen degeneration of cartilage in the knee: data from the osteoarthritis initiative. Sci Rep 6:21415
Mow VC, Kuei SC, Lai WM, Armstrong CG (1980) Biphasic creep and stress relaxation of articular cartilage in compression? Theory and experiments. J Biomech Eng 102:73–84
Pena E, Calvo B, Martinez MA, Palanca D, Doblare M (2005) Finite element analysis of the effect of meniscal tears and meniscectomies on human knee biomechanics. Clin Biomech 20:498–507
Penrose JM, Holt GM, Beaugonin M, Hose DR (2002) Development of an accurate three-dimensional finite element knee model. Comput Methods Biomech Biomed Eng 5:291–300
Poh SY, Yew KS, Wong PL, Koh SB, Chia SL, Fook-Chong S, Howe TS (2012) Role of the anterior intermeniscal ligament in tibiofemoral contact mechanics during axial joint loading. Knee 19:135–139
Proctor CS, Schmidt MB, Whipple RR, Kelly MA, Mow VC (1989) Material properties of the normal medial bovine meniscus. J Orthop Res 7:771–782
Schinagl RM, Gurskis D, Chen AC, Sah RL (1997) Depth-dependent confined compression modulus of full-thickness bovine articular cartilage. J Orthop Res 15:499–506
Schmidt-Baldassari M (2003) Numerical concepts for rate-independent single crystal plasticity. Comput Methods Appl Mech Eng 192:1261–1280
Schroeder MJ (2010) A computational framework to evaluate the efficacy of anterior cruciate ligament reconstruction procedures. Northwestern University
Schroeder MJ (2014) A multi-domain synthesis of neuromechanical adaptations post anterior cruciate ligament reconstructive surgery. Northwestern University
Seitz A, Kasisari R, Claes L, Ignatius A, Durselen L (2012) Forces acting on the anterior meniscotibial ligaments. Knee Surg Sports Traumatol Arthrosc 20:1488–1495
Sgaglione NA (2003) The biological treatment of focal articular cartilage lesions in the knee: future trends? Arthroscopy 19:154–160
Shirazi R, Shirazi-Adl A (2005) Analysis of articular cartilage as a composite using nonlinear membrane elements for collagen fibrils. Med Eng Phys 27:827–835
Shirazi R, Shirazi-Adl A (2009) Analysis of partial meniscectomy and ACL reconstruction in knee joint biomechanics under a combined loading. Clin Biomech 24:755–761
Shirazi R, Shirazi-Adl A, Hurtig M (2008) Role of cartilage collagen fibrils networks in knee joint biomechanics under compression. J Biomech 41:3340–3348
Skaggs D, Warden W, Mow V (1994) Radial tie fibers influence the tensile properties of the bovine medial meniscus. J Orthop Res 12:176–185
Sverdlik A, Lanir Y (2002) Time-dependent mechanical behavior of sheep digital tendons, including the effects of preconditioning. J Biomech Eng 124:78–84
Tang H, Buehler MJ, Moran B (2009) A constitutive model of soft tissue: from nanoscale collagen to tissue continuum. Ann Biomed Eng 37:1117–1130
Tang Y, Ballarini R, Buehler MJ, Eppell SJ (2010) Deformation micromechanisms of collagen fibrils under uniaxial tension. J R Soc Interface 7:839–850
Tiku ML, Madhan B (2016) Preserving the longevity of long-lived type II collagen and its implication for cartilage therapeutics. Ageing Res Rev 28:62–71
Tissakht M, Ahmed A (1995) Tensile stress-strain characteristics of the human meniscal material. J Biomech 28:411–422
Tyyni A, Karlsson J (2000) Biological treatment of joint cartilage damage. Scand J Med Sci Sports 10:249–265
Walker PS, Erkman MJ (1975) The role of the menisci in force transmission across the knee. Clin Orthop Relat Res 109:184–192
Wallace IJ et al (2017) Knee osteoarthritis has doubled in prevalence since the mid-20th century. Proc Natl Acad Sci 114:9332–9336
Wilson W, van Donkelaar CC, van Rietbergen B, Ito K, Huiskes R (2004) Stresses in the local collagen network of articular cartilage: a poroviscoelastic fibril-reinforced finite element study. J Biomech 37:357–366
Wilson W, van Burken C, van Donkelaar C, Buma P, van Rietbergen B, Huiskes R (2006) Causes of mechanically induced collagen damage in articular cartilage. J Orthop Res 24:220–228
Yao J, Funkenbusch PD, Snibbe J, Maloney M, Lerner AL (2006) Sensitivities of medial meniscal motion and deformation to material properties of articular cartilage, meniscus and meniscal attachments using design of experiments methods. J Biomech Eng 128:399–408